

Effects of Ionospheric Variability on Salinity and Soil Moisture Sensing Using a Spaceborne Conically- Scanning Radiometer System

Eni G. Njoku and Mahta Moghaddam

*Jet Propulsion Laboratory, M/S 300-233
4800 Oak Grove Drive, Pasadena, CA 91109
Phone: (818) 453-3693
Fax: (818) 354-9476
E-mail: eni.g.njoku@jpl.nasa.gov*

*Jet Propulsion Laboratory
California Institute of Technology
Pasadena, CA*

Abstract. Radiometers operating in the 1–3 GHz frequency range have been studied as a means for observing ocean salinity and soil moisture globally from space. Faraday rotation effects can severely limit the accuracy of these observations. In this paper the spatial and temporal characteristics of brightness temperature errors due to ionospheric variability have been investigated. A specific sensor configuration is considered, designed for ocean salinity and soil moisture sensing. The sensor is polar-orbiting, with conically scanned antenna beams at a fixed incidence angle, operating at 1.4 and 2.7 GHz. Brightness temperature errors at 1.4 GHz ranging from ~1 K at pre-dawn to >6 K in the early afternoon can be expected near peaks in the solar cycle. The brightness temperature errors can potentially be reduced to <0.2 K and <1 K, respectively, by using externally-provided information on ionospheric total electron content (TEC) from GPS satellites and modeling. The spatial and temporal patterns of the errors are determined by the Earth's magnetic field and the diurnal and interannual patterns of the ionospheric TEC, and must be accounted for in the error budgets of future ocean salinity and soil moisture missions. The use of radiometric polarimetry to directly measure the Faraday rotation may provide a means for reducing the errors to more acceptable levels than can be achieved using TEC measurements alone.

1. Introduction

Most microwave radiometers launched to date for Earth surface sensing have operated in the 6 to 90 GHz frequency range. These include the Scanning Multichannel Microwave Radiometer (SMMR) launched in 1978 on the Seasat and Nimbus-7 satellites, the Special Sensor Microwave Imagers (SSM/Is) now operating on the DMSP series of satellites, and the Advanced Microwave Scanning Radiometers (AMSRs) planned for launch on the ADEOS-II and EOS-PM1 satellites in late 2000. The 6 to 90 GHz range is not suitable for some applications, however, such as ocean salinity and soil moisture sensing. For these applications, measurements at lower frequencies in the 1–3 GHz range are necessary to obtain sufficient sensitivity to the geophysical parameters in the presence of sensor and geophysical noise.

For observations over the oceans, the ionic conductivity of sea water has a detectable and increasing effect on the ocean emissivity at frequencies below 3 GHz. The effects of ocean wind speed and temperature on emissivity decrease at these frequencies. It is thus possible to detect ocean salinity variations, in the presence of wind speed and temperature variability, at frequencies below 3 GHz. Over land, the penetration depth in soil increases with wavelength, and the effects of vegetation and surface roughness decrease with wavelength. Thus, it is possible to detect soil moisture variations in the top 2–5-cm layer, in the presence of increasing vegetation cover, at frequencies below 3 GHz. However, at frequencies below 1 GHz, the effects of galactic noise and Faraday rotation can become excessively large, decreasing the accuracies with which ocean salinity and soil moisture can

be detected. For these reasons, the 1–3 GHz frequency range is usually considered optimum for ocean salinity and soil moisture sensing from space. Several concepts have been proposed for spaceborne sensors operating in this range [Swift and McIntosh, 1983; LeVine *et al.*, 1989; Njoku *et al.*, 1999a,b]. Even in this frequency range, however, Faraday rotation is a significant source of error under certain viewing configurations, particularly for ocean salinity sensing, and its effects must be carefully evaluated.

Faraday rotation is a phenomenon that affects electromagnetic radiation as it propagates through the ionosphere. The ionosphere is generally defined as that part of the upper atmosphere where sufficient ionization exists to influence the propagation of radio waves [Davies, 1990]. The ionosphere acts as a plasma which, in the presence of the Earth's magnetic field, induces a rotation of the polarization of electromagnetic radiation propagating through it. The polarization of radiation received by a spaceborne antenna is thus rotated with respect to the polarization of the radiation emitted or scattered from the Earth's surface. The magnitude of this Faraday rotation varies inversely as the square of frequency, and becomes a significant factor in surface remote sensing at frequencies below about 5 GHz. If uncorrected, errors in estimating polarized surface brightness temperatures, caused by Faraday rotation, can lead to large errors in the retrieval of geophysical parameters.

For a microwave sensor on a polar-orbiting spacecraft the Faraday rotation depends on the spacecraft orbital position relative to the Earth's ionosphere and magnetic field, and the sensor viewing angle relative to nadir and the magnetic field. The variability of the ionospheric electron content depends on the solar angle and solar activity (diurnal, seasonal, and sunspot cycles). Reference models of the Earth's ionosphere and magnetic field [Bilitza *et al.*, 1993; Langel, 1991] can be used to compute the general characteristics of the effects of Faraday rotation on brightness temperature. These models can be augmented with real-time ionospheric measurements, such as from the Global Positioning System (GPS) network [Wilson *et al.*, 1995], to provide more accurate predictions of Faraday-induced brightness temperature errors for given locations and times.

An earlier study [LeVine and Kao, 1997] showed that a sensor in low Earth orbit operating at 1.4 GHz can experience up to 6° of Faraday rotation under solar maximum conditions even at 6 am local time when the ionospheric electron content is near its diurnal minimum. A much larger rotation occurs in the early afternoon when the electron content is at a maximum. A Faraday rotation of 6° leads to an error of ~1 K in the measured surface brightness temperature at 40° incidence angle, while brightness temperature errors of greater than 5 K can result from the larger Faraday rotation during daytime hours. These errors have significant impacts on the geophysical retrievals, especially for ocean salinity. Some correction for the errors can be made by using estimates of Faraday rotation derived from models and real-time ionospheric measurements. The uncertainties of these corrections can be estimated, and their influence on the geophysical retrievals determined.

In this paper, we extend the work of *LeVine and Kao [1997]* by considering the effects of Faraday rotation on conically-scanning or conical-pushbroom type radiometer systems operating at 1.4 and 2.69 GHz. Such systems, for ocean salinity and soil moisture sensing, have been discussed recently by *Njoku et al. [1999a,b]*. The antenna beams intersect the Earth at a constant incidence angle across the swath, with dual-polarization capability. For this type of sensor, operating in polar low Earth orbit, we have simulated typical spatial and temporal variabilities of the Faraday rotation angle Ω , and the resulting errors in satellite-observed brightness temperatures. The feasibility of estimating Ω using measurements from the current network of GPS sensors has been investigated, and the corresponding impact on the uncertainty of estimating soil moisture and ocean salinity has been evaluated. The spatial and temporal characteristics of these errors are particularly important in developing realistic error budgets for the spaceborne missions.

2. Faraday Rotation

To place in context the equations and approximations used in the following sections a brief summary of Faraday rotation is given here. The ionosphere extends from about 50 km to more than 1000 km above the Earth's surface. In this region, incident solar radiation ionizes the neutral atmosphere forming a plasma. The equilibrium between ionization and recombination results in a vertical profile of electron density $N(h)$ which varies with height h above the surface. The profile typically peaks in the F region, near $h = 300$ km, and varies with latitude and diurnal, seasonal, and sunspot cycles [*Davies, 1990*]. Electromagnetic radiation propagating through the ionosphere is subject to scattering, absorption, group delay, and Faraday rotation. Of these effects, only Faraday rotation poses a significant problem for passive sensing at 1–3 GHz. The other effects are usually too small to be detected at frequencies above 1 GHz.

When an external magnetic field \mathbf{B} is applied to a plasma it becomes electrically anisotropic. Specifically, the ionosphere in the presence of the Earth's magnetic field is a gyrotropic medium. The impermeittivity tensor for a plasma with an applied magnetic field in the z -direction can be written as

$$\kappa = \begin{bmatrix} \kappa & i\kappa_g & 0 \\ -i\kappa_g & \kappa & 0 \\ 0 & 0 & \kappa_z \end{bmatrix} \quad (1)$$

where κ , κ_g , and κ_z are functions of the plasma and cyclotron angular frequencies ω_p and ω_c , respectively [*Kong, 1990*].

In a gyrotropic medium, electromagnetic waves propagate in two characteristic modes, Type I and Type II waves, with different phase velocities. In a general direction of propagation these waves are elliptically polarized. A linearly-polarized wave entering this

medium decomposes into the Type I and Type II waves. For the special case of propagation in a direction parallel to the magnetic field (longitudinal propagation) the Type I and Type II waves are left-hand and right-hand circularly polarized (LHCP and RHCP), respectively. In propagating a distance dz in the positive z -direction, these waves are phase-shifted by different amounts ϕ_I and ϕ_{II} :

$$\phi_I = \frac{\omega dz}{\sqrt{\frac{1}{\mu_0}(\kappa + \kappa_g)}} ; \quad \phi_{II} = \frac{\omega dz}{\sqrt{\frac{1}{\mu_0}(\kappa - \kappa_g)}} ; \quad (2)$$

where ω is the angular frequency of the radiation and μ_0 is the permeability of free space. The superposition of the two waves is a linearly polarized wave whose direction of polarization rotates as the wave propagates. The amount of rotation over distance dz is given by $d\Omega = \frac{1}{2} (\phi_{II} - \phi_I)$ (radians). The sense of the rotation is clockwise for an observer viewing in the negative z -direction. (The rotation is also clockwise, from the same viewpoint, for a wave traveling in the negative z -direction.) At frequencies above 1 GHz, and for representative ionospheric and magnetic field conditions, the frequency is much higher than the plasma and cyclotron frequencies, i.e. $\omega \gg \omega_p$, and $\omega \gg \omega_c$. This allows approximations for κ , κ_g , and κ_z to be made [Kong, 1990] such that the magnitude of the Faraday rotation over distance dz can be expressed as

$$d\Omega = \frac{\omega_c \omega_p^2}{2 c \omega^2} dz = K \frac{N B_0}{f^2} dz \quad (3)$$

where c is the speed of light, and the standard expressions have been substituted for ω_p and ω_c . $B_0 = |B|$ is the magnitude of the Earth's magnetic field in tesla, and f is the frequency in Hz. For N in m^{-3} and dz in meters, the constant K has the value 2.365×10^4 .

As stated above, Equation (3) assumes longitudinal propagation. For the general case of propagation at an angle α to the magnetic field a 'quasi-longitudinal' approximation [Davies, 1990] can be derived which holds if the following condition is satisfied:

$$(Y \sin \alpha)^4 \ll 4 (1 - X)^2 (Y \cos \alpha)^2 \quad (4)$$

where, $Y = \omega_c/\omega$ and $X = \omega_p^2/\omega^2$. For frequencies above 1 GHz this condition is satisfied when $0^\circ < \alpha < 89.9^\circ$, i.e. the approximation is valid except for propagation directly perpendicular to the magnetic field. The approximation results in an expression similar to Equation (3), but where dz is replaced by $dz \cos \alpha$. Using this expression, and integrating along a slant propagation path from the surface to the satellite, the total Faraday rotation along the path is

$$\Omega = \frac{K}{f^2} \int_0^H N B_0 \cos \alpha \sec \chi \, dh \quad (5)$$

where χ is the angle between the propagation path and the vertical, and H is the satellite altitude. The parameters N , B_0 , α , and χ are functions of altitude h . Equation (5) is a commonly used expression for Faraday rotation. The expression can also be written as

$$\Omega = \frac{K}{f^2} \bar{M} N_T \quad (6)$$

where N_T (m^{-2}) is the total electron content (TEC) at height H (i.e. the integral of N from the surface to height H), and $\bar{M} = B_0 \cos \alpha \sec \chi$ is the magnetic field factor along the path, i.e.

$$N_T = \int_0^H N \, dh \quad (7)$$

$$\bar{M} = \frac{1}{N_T} \int_0^H N B_0 \cos \alpha \sec \chi \, dh \quad (8)$$

Equation (5) provides a means for computing the Faraday rotation angle for a given sensor viewing configuration, provided the magnetic field and ionospheric electron content are known as functions of altitude along the observation path. In the next section models of the Earth's magnetic field and electron density profiles are used to compute Ω for a variety of observational configurations. These models are used for simulation only. If the electron density profile $N(h)$ is not known, but the total electron content N_T is known, then Equation (6) provides a means for estimating Ω if a good estimate of \bar{M} can be made. This will be discussed in a later section.

3. Magnetic Field and Ionospheric Models

Magnetic Field

To first order, the Earth's magnetic field can be approximated as the field of a magnetic dipole located at the Earth's center with its axis inclined to the Earth's rotational axis. The magnitude of the field and the inclination of its axis relative to the Earth's rotational axis vary slowly with time. The plane through the Earth's center, perpendicular to the dipole axis, is the dipole equator. The dipole latitude Φ is expressed relative to the dipole equator.

The dipole field \mathbf{B} , at a point P with coordinates (r, Φ) at a radial distance r from the Earth's center, is given by

$$\mathbf{B} = -B_g \left(\frac{R}{r}\right)^3 [\hat{\mathbf{i}}_t \cos\Phi + \hat{\mathbf{i}}_z 2 \sin\Phi] \quad (9)$$

where $R \equiv 6378$ km is the Earth's radius, $B_g \equiv 0.31 \times 10^{-4}$ tesla is the magnetic field strength on the Earth's surface at the dipole equator, $\hat{\mathbf{i}}_t$ is the unit vector tangential to the magnetic field at P (pointing to geomagnetic north), and $\hat{\mathbf{i}}_z$ is the unit vector in the radial direction at P (pointing inward).

The Earth's magnetic field can be modeled more accurately by using a spherical harmonics representation with available geomagnetic measurement data. The International Geomagnetic Reference Field (IGRF) [Langel, 1991] is the model recommended for use by the International Association of Geomagnetism and Aeronomy (IAGA). The IGRF model is available from the NASA Goddard Space Flight Center (GSFC) National Space Science Data Center (NSSDC) as a software package that allows the Earth's magnetic field components to be computed as a function of location and time. Figure 1 shows the field magnitude B_0 for the year 1994 at an altitude of $h = 300$ km. This altitude is near the peak of the electron density profiles. The region of the ionosphere around this altitude provides the dominant contribution to the Faraday rotation. As can be seen, the magnetic field deviates significantly from the simple dipole field of Equation (9).

Ionosphere

Several models have been developed from which representative ionospheric electron density profiles can be computed as functions of location and time. One of the most comprehensive sets of models is the International Reference Ionosphere (IRI) [Bilitza *et al.*, 1993] sponsored by the Committee for Space Research (COSPAR) and the International Union of Radio Science (URSI). The models include data from the worldwide ionosonde network, incoherent scatter radars, satellite sounders, and in situ sensors. The IRI software, available from the NSSDC, can be used to display pertinent characteristics of the profiles $N(h)$ and the total electron content N_T .

Figure 2 shows representative profiles using the IRI model for different latitudes (0° and 60°N), local times (noon and midnight at 0° longitude), and seasons (January 30 and July 30, 1994). 1994 was a year of moderate solar activity, midway between the sunspot maximum in 1990–91 and minimum in 1996–7. The profiles exhibit a characteristic peak. The peak varies in magnitude and altitude depending on the latitude, local time, and season. The midday values are higher than the midnight values as expected due to solar ionization effects.

The time-variability of the total electron content N_T is shown in Figures 3 and 4. Figure 3 shows the variation of N_T over a diurnal cycle, computed for an altitude of 700

km, 0° longitude, and latitudes between 60°N and 60°S (1 TEC unit = 10^{16} m^{-2}). Minimum and maximum values of N_T tend to occur near 4–5 am and 1 pm local times, respectively, although in some cases the maxima are broad and may have local minima. Figure 4 shows the variation of N_T over a 15-year period computed at UT12 on January 30 each year, and illustrates the effect of the approximately 11-year sunspot cycle. The spatial variability of N_T (at an altitude of 700 km) is shown in Figures 5(a)–(d) for January 30, 1990. The maps show the distributions of N_T at four times of day: UT00, 06, 12, and 18. The distributions do not exhibit a simple solar-angle dependence on latitude and longitude due to the complex mechanisms of ion formation, recombination, and transport in the ionosphere.

4. Faraday Rotation Computations

The IGRF and IRI models have been used to simulate the global variation of the Faraday rotation angle Ω , for particular ionospheric conditions and for the sensor orbit and viewing configurations of a generic soil moisture and ocean salinity satellite system similar to that described by *Njoku et al.* [1999a,b], as listed in Table 1. The orbit is assumed to be polar and sun-synchronous with an altitude of 700 km and nodal equator crossings at 6 am and 6 pm local time. The antenna beams are assumed to have a conical-pushbroom or conical-scanning configuration with an incidence angle of 40° . This provides a swath width of approximately 1000 km, with global coverage between 85°N and 85°S at least every three days. The study focuses on 1.41 and 2.69 GHz since these frequencies are suitable for soil moisture and ocean salinity sensing and are in bands allocated for passive sensing [Litman and Nicholas, 1982]. Observations are assumed to be made at vertical and horizontal polarizations at each frequency.

Table 1: Orbital and sensor viewing characteristics assumed for Faraday rotation computations

Operating Frequencies (GHz)	1.41	2.69
Polarizations	V, H	V, H
Orbit altitude (km)	700	
Orbit inclination (deg)	98.2	
Nodal equator crossings	6am/6pm	
Incidence angle (deg)	40	
Swath width (km)	1020	
Global coverage period (days)	3	

Magnetic Field Factor Approximation

To avoid the complexity of computing the integral in Equation (5) for the varying orbit positions and antenna viewing directions, we have used Equation (6) with an expression for the approximate magnetic field factor \bar{M} . This allows the total electron content N_T to be used rather than the detailed profiles $N(h)$ in the computations and correction procedures. The expression for \bar{M} can be derived from Equation (8) by noting that the electron density profiles (Figure 2) represent peaked weighting functions with significant values generally in the $h = 150\text{--}600$ km range, while the magnetic field (which has an approximately r^3 radial dependence with origin at the Earth's center) is slowly varying over this altitude range. Thus, the weighting functions effectively select out the value of M in the integrand at the altitudes of the weighting function peaks. Equation (8) can therefore be rewritten as

$$\bar{M} = \frac{1}{N_T} \int_0^H N \mathbf{B} \cdot \hat{\mathbf{i}}_s \sec\chi \, dh \equiv \left[\mathbf{B} \cdot \hat{\mathbf{i}}_s \sec\chi \right]_{h=h_0} \quad (10)$$

where the expression in square brackets is evaluated at the peak altitude h_0 of the weighting function, $\mathbf{B} = B_0 \hat{\mathbf{i}}_b$ is the magnetic field vector, $\hat{\mathbf{i}}_b$ is a unit vector in the direction of the magnetic field, $\hat{\mathbf{i}}_s$ is a unit vector in the antenna viewing direction, and $\hat{\mathbf{i}}_b \cdot \hat{\mathbf{i}}_s = \cos \alpha$. In the general case h_0 is unknown, however a fixed value can be used with little error. For example, for the profiles of Figure 2, which are representative of a full range of geographic and seasonal variation, using a value of $h_0 = 360$ km to evaluate the right hand side of Equation (10) for all the profiles shown results in a maximum error for \bar{M} of 2.5%. This is adequate for the purposes here.

Equations (6) and (10) were used, with $h_0 = 360$ km, to compute global maps of Faraday rotation angle Ω based on the IGRF and IRI reference fields. For the assumed sensor configuration, a constant value of 40° for the nadir viewing angle χ was used (Table 1). However, for any given position (i.e. latitude and longitude) in the satellite orbit at which \bar{M} is being computed the angle α varies as a function of the antenna boresight direction (specified by χ and the azimuth angle β) and the magnetic field direction (see Figure 6). We note that

$$\mathbf{B} \cdot \hat{\mathbf{i}}_s = B_x \sin\chi \cos\beta + B_y \sin\chi \sin\beta + B_z \cos\chi \quad (11)$$

For each latitude and longitude the maximum and minimum values $|\Omega|_{\max}$ and $|\Omega|_{\min}$ of the magnitude of the Faraday rotation angle were computed, as the azimuth angle β was varied from 0 to 360° to simulate the antenna scan of the spaceborne sensor. Figure 7 shows the spatial variation of $|\Omega|_{\max}$ and $|\Omega|_{\min}$ at 1.41 GHz at two times of day (UT06 and UT18 on July 30, 1990). The spatial variations of the Faraday rotation angle follow the variations of the magnetic field (Figure 1) and total electron content (Figure 5), combined according to Equations 6 and 10. At 6 am local time (UT06 at longitude 0° , and

UT18 at longitude 180°E) the maximum Faraday rotation is less than 6–8° except near the poles, while at 6 pm local time (UT18 at longitude 0°, and UT06 at longitude 180°E) the maximum Faraday rotation reaches ~15° near the equator. Figure 7 represents a snapshot, for a given month and year, of the spatial variability of the Faraday rotation for the conically scanning radiometer being considered.

Brightness Temperature Error and Impact on Surface Parameter Estimation

The effect of the Faraday rotation on the satellite-observed brightness temperatures can be expressed as [Njoku, 1980]

$$\begin{bmatrix} T_{B_v}' \\ T_{B_h}' \end{bmatrix} = \begin{bmatrix} \cos^2\Omega & \sin^2\Omega \\ \sin^2\Omega & \cos^2\Omega \end{bmatrix} \begin{bmatrix} T_{B_v} \\ T_{B_h} \end{bmatrix} \quad (12)$$

or, in matrix notation

$$\mathbf{T}_B' = \mathbf{Q}(\Omega) \cdot \mathbf{T}_B \quad (13)$$

where T_{B_v}' and T_{B_h}' are the brightness temperatures measured at the vertical and horizontal ports of the satellite antenna. T_{B_v} and T_{B_h} are the surface brightness temperatures at vertical and horizontal polarizations, and $\mathbf{Q}(\Omega)$ is the Faraday rotation matrix. The error in neglecting the Faraday rotation is $\Delta\mathbf{T}_B = \mathbf{T}_B' - \mathbf{T}_B = [\mathbf{Q}(\Omega) - \mathbf{I}] \cdot \mathbf{T}_B$, which can be written as

$$\Delta T_{B_v} = -\Delta T_{B_h} = -\sin^2\Omega (T_{B_v} - T_{B_h}) \quad (14)$$

The difference $(T_{B_v} - T_{B_h})$ between the vertical and horizontal polarized brightness temperatures depends on the surface type and the atmospheric conditions. Atmospheric effects are small below 3 GHz. Over calm oceans and bare-soil surfaces the brightness temperature polarization difference can be 50 K or larger at an incidence angle of 40°. Over thickly vegetated surfaces the polarization difference can decrease to near 0 K. Thus, from Equation (14), worst-case brightness temperature errors of ~1 K at 6 am, and ~3.4 K at 6 pm, local times, can be anticipated for Faraday rotations of 8° and 15°, respectively. Note that these errors have been computed using the IGRF and IRI reference fields for January 1990, which is a northern-hemisphere winter season near a peak of the sunspot cycle (Figure 4). Smaller errors will be encountered for years of reduced solar activity, with the errors scaling approximately proportionally to N_T .

A 6-am brightness temperature error of ~1 K is tolerable for soil moisture sensing. However, an error of this magnitude is unacceptable for ocean salinity sensing, for which brightness temperature accuracies of better than 0.2 K are desired. Some form of Faraday

rotation is necessary for salinity sensing to be feasible, and if data during other times of day (e.g. 6 pm) are to be useful for soil moisture sensing.

The brightness temperature error due to Faraday rotation can be corrected to some extent if estimates of Ω are available. An estimate of Ω can be written as $\Omega^* = \Omega + \Delta\Omega$, where $\Delta\Omega$ is the error in the estimate. A correction for the brightness temperature can then be written as the inverse of Equation (13), $T_B^* = Q(\Omega^*)^{-1} \cdot T_B'$, and the error in the correction is then $\Delta T_B = \varepsilon \cdot T_B$, where

$$\varepsilon = [Q(\Omega^*)^{-1} \cdot Q(\Omega) - I] \quad (15)$$

Evaluation of ε for small $\Delta\Omega$ gives the error in the corrected brightness temperatures as

$$\Delta T_{B_v} = -\Delta T_{B_h} = \Delta\Omega \tan 2\Omega (T_{B_v} - T_{B_h}) \quad (16)$$

Figure 8 shows maps of $|\Delta T_B|$ for both the uncorrected and corrected cases, computed from Equations (14) and (16) respectively. A brightness temperature polarization difference of 50 K and an uncertainty in total electron content of 3 TEC units (for estimating $\Delta\Omega$) have been assumed. The corrections are seen to reduce the brightness temperature errors to less than 0.2 K at 6 am, except near the poles, and less than 0.5 K at 6 pm, for the month and year shown. This is sufficient for soil moisture sensing, but marginal for salinity sensing even at 6 am. For salinity sensing, other more accurate correction methods are desirable. Polarimetric methods, in which measurements of the third Stokes parameter are made in conjunction with the vertical and horizontal brightness temperature measurements, offer one such possibility.

The error distributions shown in Figure 8 are representative only, and are based on modeled total electron content distributions. They provide a reasonably accurate assessment of the spatial and temporal variability of the Faraday rotation-induced errors. Error distributions for a frequency of 2.7 GHz can be obtained by a simple scaling of the 1.4 GHz distributions by a factor of $(1.4/2.7)^2$, i.e. by a factor of approximately 0.3.

Accuracy of Corrections

The assumption of 3 TEC units uncertainty in N_T for the corrections to ΔT_B is somewhat optimistic given the current state-of-the-art in estimating global total electron content. Recent work [Wilson *et al.*, 1995] has shown that maps of total electron content (TEC) can be derived in near real-time from the world-wide network of GPS receivers. The GPS TEC measurements have been compared directly with radar altimeter (TOPEX) measurements with good agreement [Ho *et al.*, 1997]. However, due to the sparse GPS receiver coverage of the equatorial and southern hemisphere regions, the GPS TEC maps are currently most useful in the latitude band 20°–80°N. In this region the maps are

considered accurate to within 5 TEC units. Over the rest of the globe TEC estimates extrapolated from retrospective data such as the IRI model must be relied upon, with lower expected accuracy. The optimistic assumption of 3 TEC units, used above, is considered a realistic projection for the coming decade as the GPS measurement network and modeling capability improves globally.

Another source of uncertainty in using GPS TEC measurements for correcting Faraday rotation is that the GPS total electron content N_T is derived at the altitude of the GPS satellites (~22,000 km). The difference between N_T at the altitude of a polar-orbiting sensor (700 km in this study) and the GPS satellite altitude can be on the order of 10–20% or more and must be estimated. One method for determining this difference precisely is to mount an upward-looking GPS receiver on the polar-orbiting satellite to provide the total electron content difference.

Perhaps the most promising method for correcting Faraday rotation is the measurement of the third Stokes parameter (U -component of the Stokes vector) along with the conventional vertical (V) and horizontal (H) brightness temperature polarizations. Assuming an azimuthally symmetric ocean surface the U , V , and H measurements can provide a direct estimate of the Faraday rotation. This approach is the subject of a separate study (S. Yueh, personal communication).

Discussion

This study was undertaken as part of a feasibility analysis of the use of L- and S-band radiometry for soil moisture and ocean salinity sensing using a conical-scan antenna system in low-Earth orbit, with orbital ground-coverage times near 6 am and 6 pm. The results of the study show that Faraday rotation is a significant error source for soil moisture sensing for the ~6 pm portion of the orbit, and for ocean salinity at all portions of the orbit. Use of GPS measurements can reduce the errors sufficiently for soil moisture sensing at any time of day, and may suffice for ocean salinity sensing using the ~6 am orbit segment during periods of low to moderate solar activity. However, for ocean salinity sensing more precise and direct measurements are desirable, such as may be provided by including polarimetric channels on the microwave radiometer. Further research on the implementation and testing of this technique is necessary.

Acknowledgments

This work was performed at the Jet Propulsion Laboratory, California Institute of Technology, Pasadena, California, under contract with the National Aeronautics and Space Administration.

References

- Bilitza, D., K. Rawer, L. Bosny, and T. Gulyaeva, International Reference Ionosphere—Past, present, future, *Adv. Space. Res.*, 13(3), 3-23, 1993.
- Davies, K., *Ionospheric Radio*, Peter Peregrinus, London, 1990.
- Ho, C. M., B. D. Wilson, A. J. Mannucci, U. J. Lindqwister, and D. N. Yuan, A comparative study of ionospheric total electron content measurements using global ionospheric maps of GPS, TOPEX radar, and the Bent model, *Radio Science*, 32(4), 1499-1512, 1997.
- Kong, J. A., *Electromagnetic Wave Theory*, Wiley-Interscience, New York, 1990.
- Langel, R. A., International Geomagnetic Reference Field, 1991 Revision, *J. Geomag. Geoelectr.*, 43, 1007-1012, 1991.
- LeVine, D. E., T. T. Wilheit, R. E. Murphy, and C. T. Swift, A multifrequency microwave radiometer of the future, *IEEE Trans. Geosci. Rem. Sens.*, 27(2), 193-199, 1989.
- LeVine, D. M. and M. Kao, Effects of Faraday rotation on microwave remote sensing from space at L-band, *Proceedings of the IEEE Geoscience and Remote Sensing Symposium*, Singapore, August 4-8, 1997.
- Litman, V. and J. Nicholas, Guidelines for spaceborne microwave remote sensors, *NASA Reference Publication RP-1086*, National Aeronautics and Space Administration, Washington, DC, 1982.
- Njoku, E. G., Antenna pattern correction procedures for the scanning multichannel microwave radiometer (SMMR), *Boundary-Layer Meteorol.*, 18, 79-98, 1980.
- Njoku, E. G., Y. Rahmat-Samii, J. Sercel, W. Wilson, and M. Moghaddam, Evaluation of an inflatable antenna concept for microwave sensing of soil moisture and ocean salinity, *IEEE Trans. Geosci. Rem. Sens.*, 37, 63-78, 1999.
- Njoku, E. G., W. J. Wilson, S. H. Yueh, and Y. Rahmat-Samii, A Large-antenna microwave radiometer-scatterometer concept for ocean salinity and soil moisture sensing, *IEEE Trans. Geosci. Rem. Sens.*, (submitted, 1999).
- Swift, C. T. and R. E. McIntosh, Considerations for microwave remote sensing of ocean surface salinity, *IEEE Trans. Geosci. Rem. Sens.*, GE-21(4), 480-491, 1983.
- Wilson, B. D., A. J. Manucci, and C. D. Edwards, Subdaily northern hemisphere ionospheric maps using an extensive network of GPS receivers, *Radio Science*, 30(3), 639-648, 1995.

Figure Captions

- Figure 1: IGRF representation of the Earth's magnetic field magnitude B_0 (in units of 10^{-4} tesla) for the year 1994 and altitude 300 km. (Grid lines are at 20° lat-lon intervals.)
- Figure 2: IRI electron density profiles for different seasons (January 30 and July 30) at noon and midnight (Universal Times UT00 and UT12 at 0° longitude) for the year 1994. (a) Latitude 0°N . (b) Latitude 60°N . Note: the horizontal scale of (a) is twice that of (b).
- Figure 3: Diurnal cycle of the total electron content N_T computed from the IRI model at an altitude of 700 km, 0° longitude, and latitudes between 60°N and 60°S . (a) January 30, 1990. (b) July 30, 1990. (1 TEC unit = 10^{16} m^{-2} .)
- Figure 4: Interannual variability of the total electron content N_T computed from the IRI model at UT12 on January 30 each year, at an altitude of 700 km, 0° longitude, and latitudes between 60°N and 60°S . (1 TEC unit = 10^{16} m^{-2} .)
- Figure 5: IRI-modeled total electron content N_T at 700 km altitude for January 30, 1990 as a function of latitude and longitude at four times of day. (a) UT00, (b) UT06, (c) UT12, (d) UT18. (Regions with N_T greater than 50 TEC units are shaded.)
- Figure 6: Geometry of the antenna beam viewing direction $\hat{\mathbf{i}}_s$ relative to the Earth's magnetic field \mathbf{B} . The direction $\hat{\mathbf{i}}_x$ points to geographic north, $\hat{\mathbf{i}}_z$ points towards nadir.
- Figure 7: Magnitude of the Faraday rotation angle $|\Omega|$ at a frequency of 1.4 GHz. Maximum and minimum values (dependent on the antenna-beam azimuth angle) are shown for two times of day on January 30, 1990. (a) Maximum, UT06; (b) Minimum, UT06; (c) Maximum, UT18; (d) Minimum, UT18. Contours are at intervals of 3° . Regions with $|\Omega|$ greater than 12° are shaded.
- Figure 8: Brightness temperature errors due to Faraday rotation, computed at a frequency of 1.4 GHz, assuming a polarization difference of 50 K. (a) Uncorrected. (b) Corrected, assuming knowledge of total electron content to within 3 TEC units. Computations are for the worst case ("Max") antenna-beam azimuth angle, and for UT06, January 30, 1990.

IGRF Model (1994, $h = 300$ km)

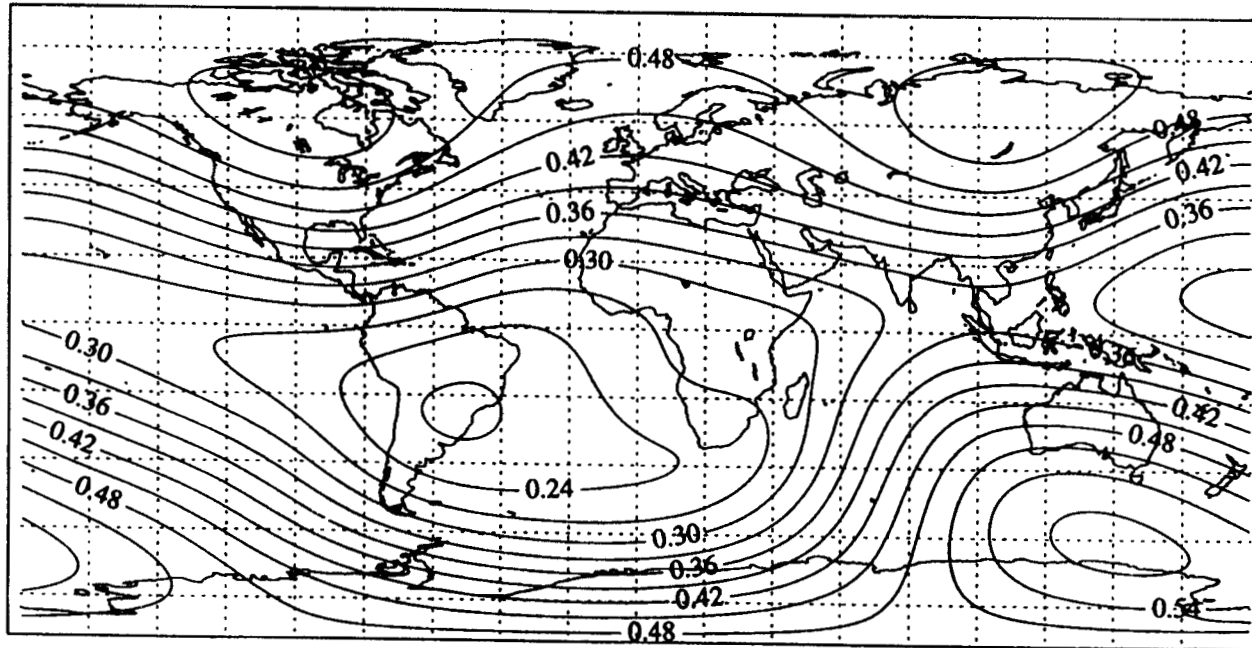


Figure 1: IGRF representation of the Earth's magnetic field magnitude B_0 (in units of 10^{-4} tesla) for the year 1994 and altitude 300 km. (Grid lines are at 20° lat-lon intervals.)

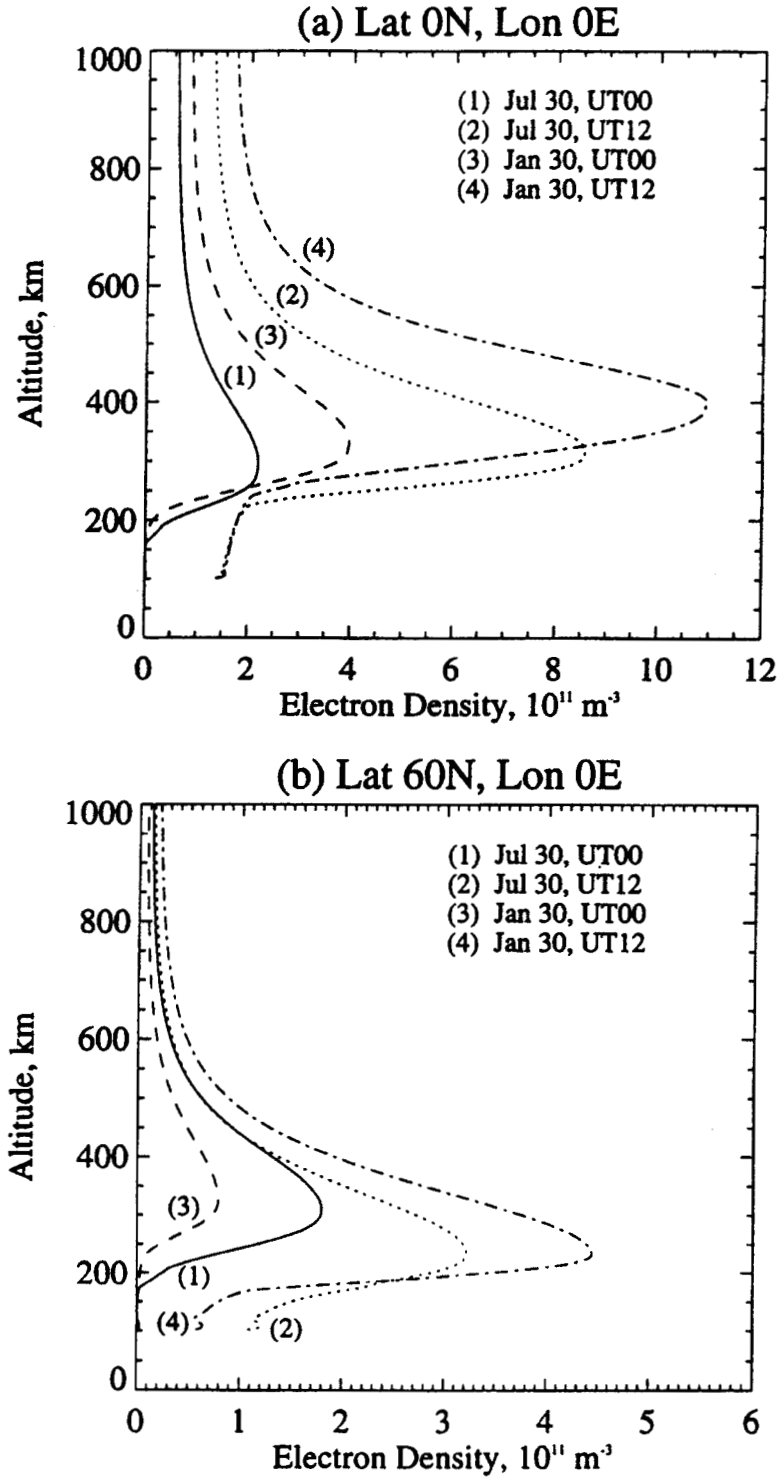


Figure 2: IRI electron density profiles for different seasons (January 30 and July 30) at noon and midnight (Universal Times UT00 and UT12 at 0° longitude) for the year 1994. (a) Latitude 0°N. (b) Latitude 60°N. Note: the horizontal scale of (a) is twice that of (b).

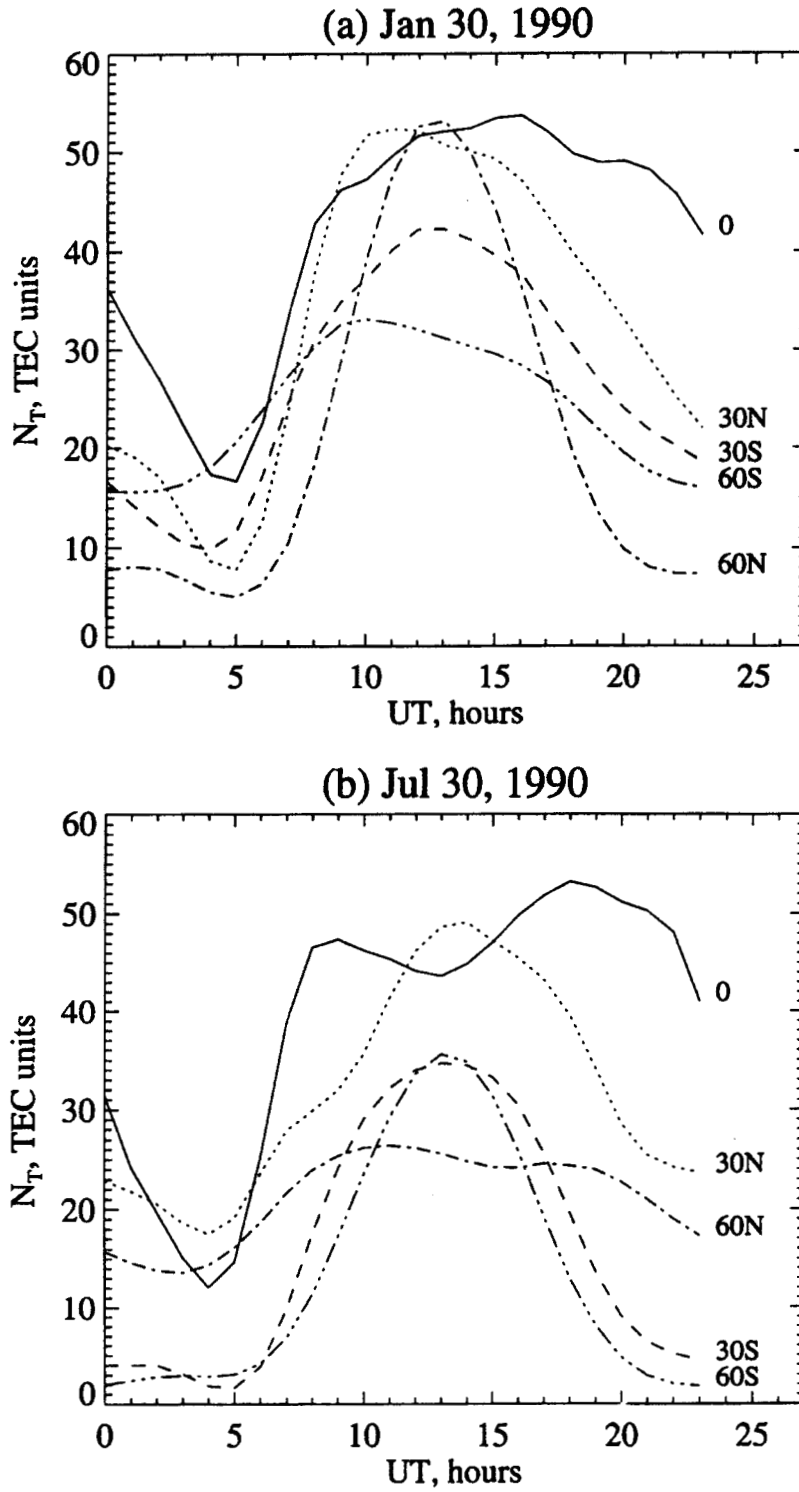


Figure 3: Diurnal cycle of the total electron content N_T , computed from the IRI model at an altitude of 700 km, 0° longitude, and latitudes between 60°N and 60°S . (a) January 30, 1990. (b) July 30, 1990. (1 TEC unit = 10^{16} m^{-2} .)

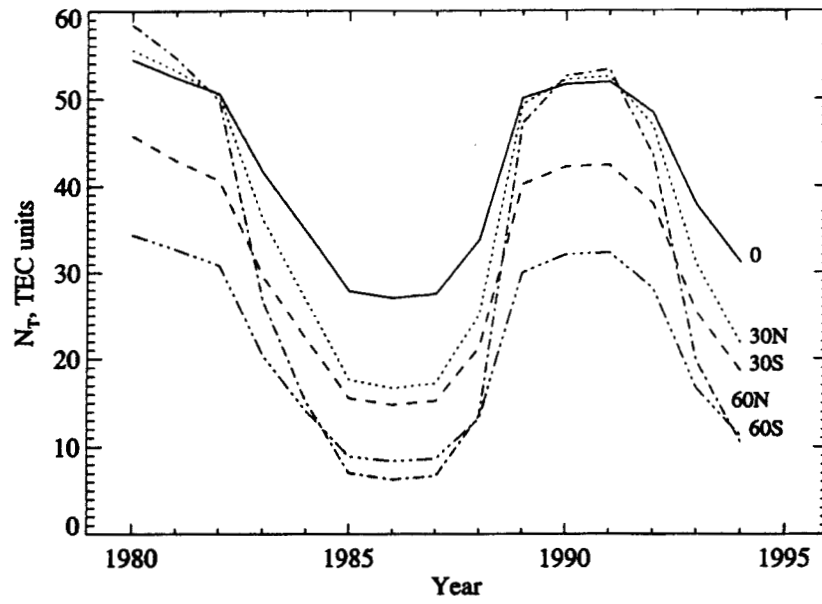


Figure 4: Interannual variability of the total electron content N_T , computed from the IRI model at UT12 on January 30 each year, at an altitude of 700 km, 0° longitude, and latitudes between 60°N and 60°S . (1 TEC unit = 10^{16} m^{-2} .)

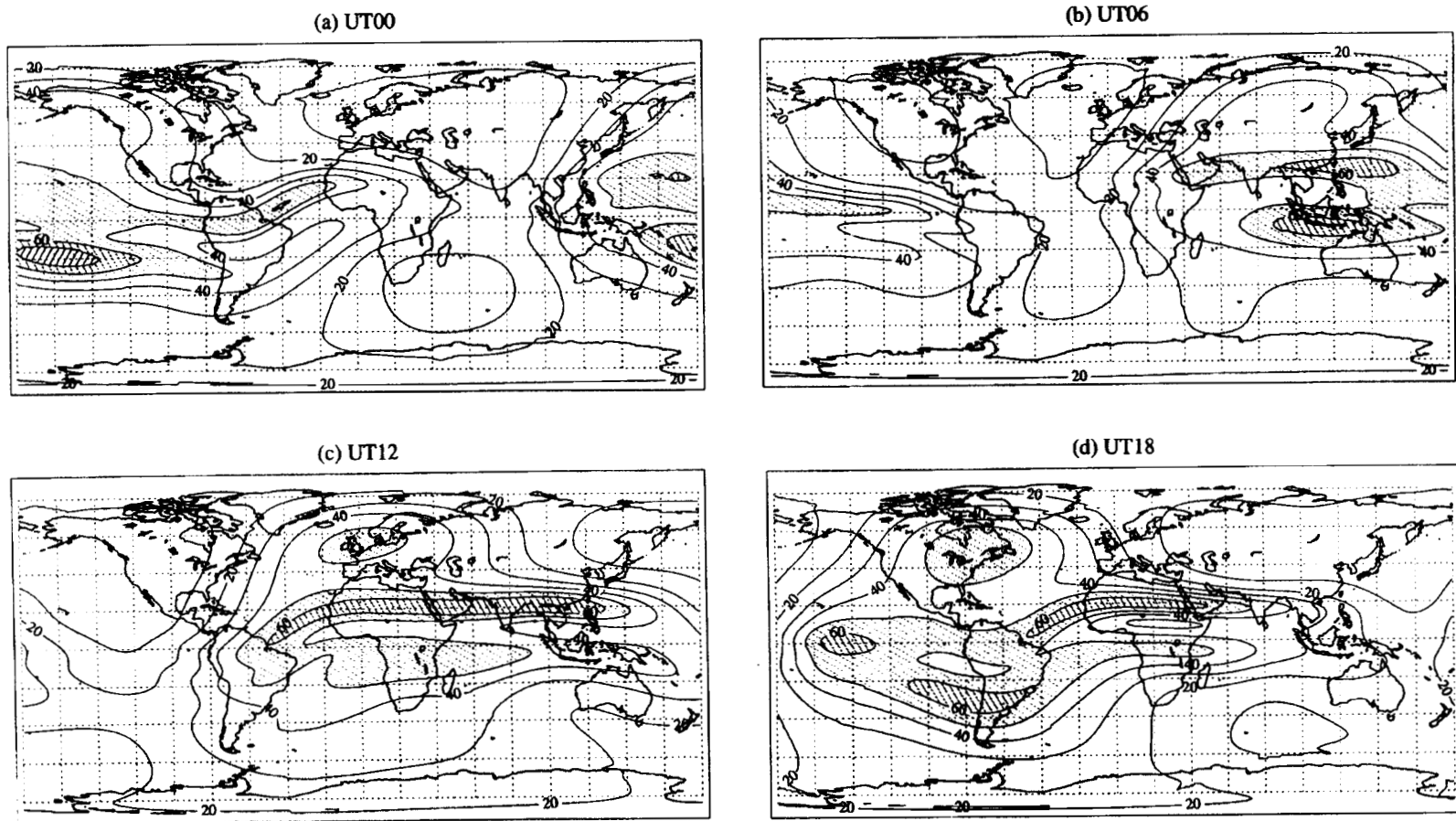


Figure 5: IRI-modeled total electron content N_T at 700-km altitude for January 30, 1990 as a function of latitude and longitude at four times of day. (a) UT00, (b) UT06, (c) UT12, (d) UT18. (Regions with N_T greater than 50 TEC units are shaded.)

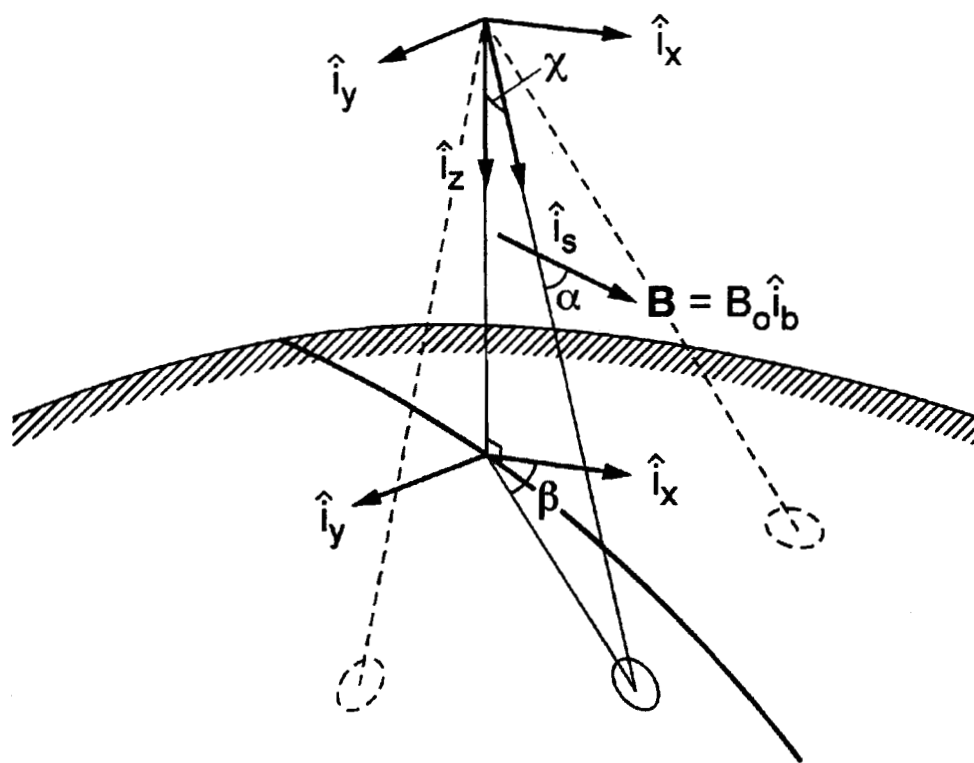


Figure 6: Geometry of the antenna beam viewing direction \hat{i}_s relative to the Earth's magnetic field \mathbf{B} . The direction \hat{i}_x points to geographic north, \hat{i}_z points towards nadir.

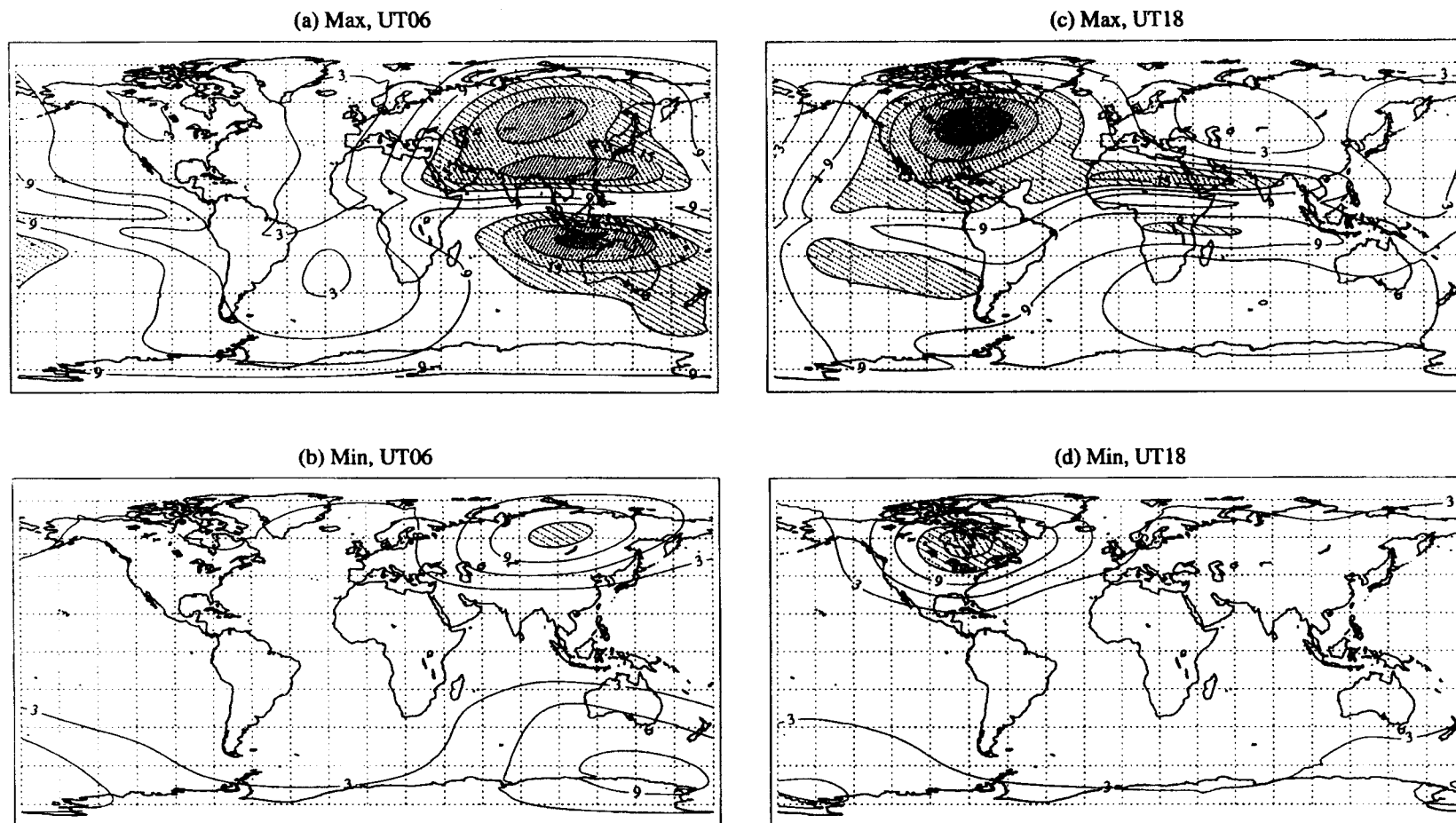


Figure 7: Magnitude of the Faraday rotation angle $|\Omega|$ at a frequency of 1.4 GHz. Maximum and minimum values (dependent on the antenna-beam azimuth angle) are shown for two times of day on January 30, 1990. (a) Maximum, UT06; (b) Minimum, UT06; (c) Maximum, UT18; (d) Minimum, UT18. Contours are at intervals of 3° . Regions with $|\Omega|$ greater than 12° are shaded.

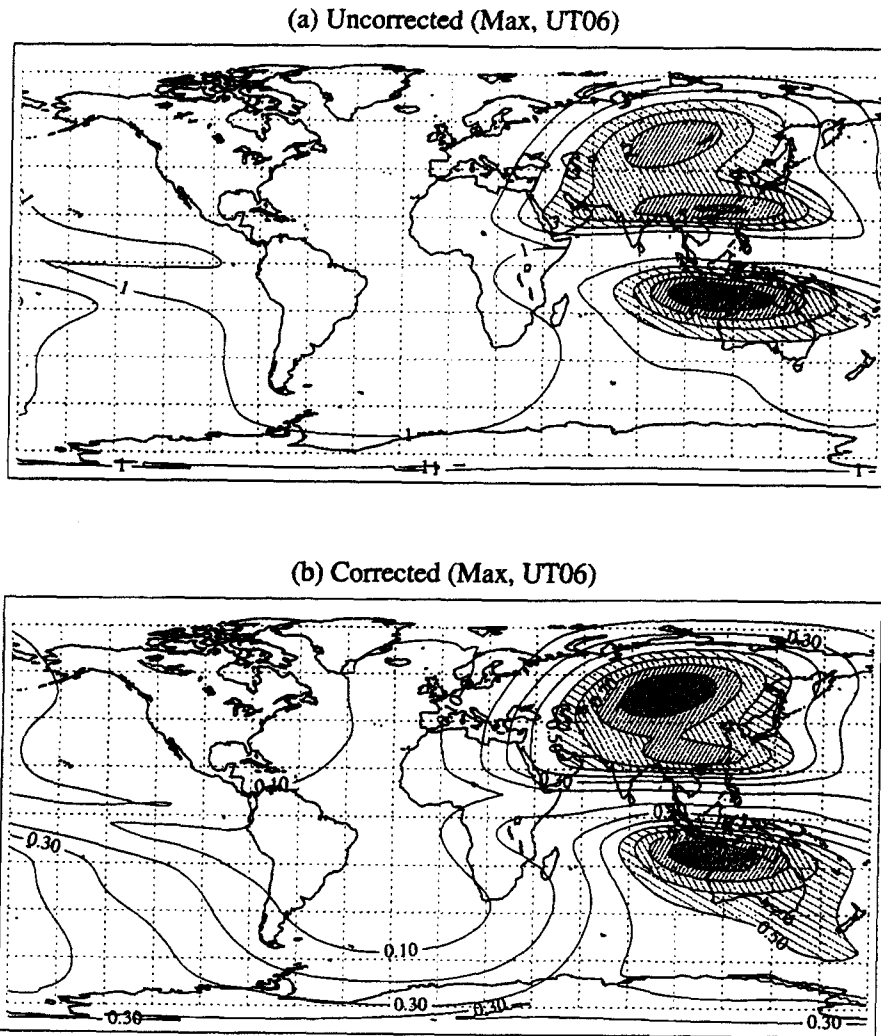


Figure 8: Brightness temperature errors due to Faraday rotation, computed at a frequency of 1.4 GHz, assuming a polarization difference of 50 K. (a) Uncorrected. (b) Corrected, assuming knowledge of total electron content to within 3 TEC units. Computations are for the worst case ("Max") antenna-beam azimuth angle, and for UT06, January 30, 1990.